Optics Letters

Ultralow-noise sub-two-cycle pulses at 1600 nm from a compact fiber-feedback optical parametric oscillator system at 76 MHz

Johann Thannheimer,[1,*] Abdullah Alabbadi,[1,2] Tobias Steinle,[1,3] and Harald Giessen[1]

[1]4th Physics Institute and Research Center SCoPE, University of Stuttgart, Stuttgart, Germany
[2]Current affiliation: Max Planck Institute for the Science of Light, Erlangen, 91058, Germany
[3]SI Stuttgart Instruments GmbH, Stuttgart, Germany
*johann.thannheimer@pi4.uni-stuttgart.de

Received 26 November 2024; revised 16 January 2025; accepted 20 January 2025; posted 21 January 2025; published 12 February 2025

We demonstrate fiber-based self-compression down to sub-two optical cycles (9.5 fs) at 1600 nm with an average power of 620 mW (8.2 nJ) and a repetition rate of 76 MHz. We use an Yb-based pump laser to drive an optical parametric oscillator, which is subsequently amplified to the watt scale using an optical parametric amplifier. The grating-free single stage pulse compression is realized by a 42-mm-long common single mode fiber. The compact system is furthermore shown to be highly stable, shot-noise-limited, and a broadband mid-infrared source through intra-pulse difference frequency generation.

https://doi.org/10.1364/OL.550337

The advent of ultrashort lasers [1–3] has opened the road toward novel spectroscopic capabilities, particularly in few-cycle pump–probe spectroscopy [4], or electro-optic sampling [5,6] for measuring the electric field evolution on even the shortest sub-cycle time scales of THz pulses [7].

Broad spectra of ultrashort pulses are particularly advantageous in ultrafast spectroscopy [8]. Time-resolved investigations of photochemical processes were enabled by such techniques [9]. Few-cycle pulses can also be used for the virtually alignment-free generation of broadband mid-infrared (MIR) radiation through intra-pulse different frequency generation (DFG) [10,11]. As most molecules have unique absorption lines in this spectral region, a broadband MIR source is the core of many molecular fingerprinting setups [12,13].

Several fiber-based compression setups that are at the heart of generating few-cycle laser pulses have been reported in the literature, e.g., fiber laser-based systems with high average power [14] or pulse durations down to a single cycle [15]. Amplified spontaneous emission inherently increases the noise level of such high-gain waveguide lasers, as amplified spontaneous emission is fed back into the laser mode [16].

A solid-state thin-disk laser in combination with a compression photonic-crystal fiber has been used in [17], where high average power at a central wavelength of 2 µm was demonstrated. As the utilized pump laser is not available commercially, this setup is hard to reproduce in other labs. Other common sources for few-cycle pulses are ultrafast noncollinear optical parametric amplifiers (NOPAs) [18,19]. They are important ultrashort light sources, but unfortunately have several drawbacks for certain applications. Their setup is quite complex, and their white light seed causes high relative intensity noise (RIN). Furthermore, even high-repetition rate NOPAs [20,21] operate usually at low single digit MHz repetition rates. Similar reasoning applies to optical parametric chirped-pulse amplifiers (OPCPAs) [22]. A fiber laser system based on commercial components is presented in [23], but the lower pulse duration limit is at about seven optical cycles. Most fiber laser-based sources are also limited in their tunability constrained by their gain bandwidth.

Therefore, the available laser sources leave open a need for a compact tunable few-cycle laser pulse source with excellent noise properties, which is readily reproducible in any ultrafast laboratory that requires such a source for the aforementioned applications. This Letter closes this gap by presenting a laser capable of generating ultralow-noise sub-two cycle pulses centered around 1600 nm using a compact fiber-based compression setup at a 76 MHz repetition rate. This is achieved using only components easily available commercially and an off-the-shelf pump laser.

The single-stage temporal compression mechanism used in this work is based on soliton self-compression and can be intuitively understood as follows: The uncompressed pulse centered at 1600 nm enters a short piece of common single-mode fiber. The fiber has a positive nonlinear refractive index and an anomalous dispersion in the spectral region above 1.3 µm. As soon as the pulse enters the fiber, self-phase modulation will cause spectral broadening and chirp the pulse in such a way that the long-wavelength components are shifted toward its leading edge, while the short wavelength components are shifted toward its trailing edge. As the anomalous dispersion slows the long-wavelength components compared to the short ones, the

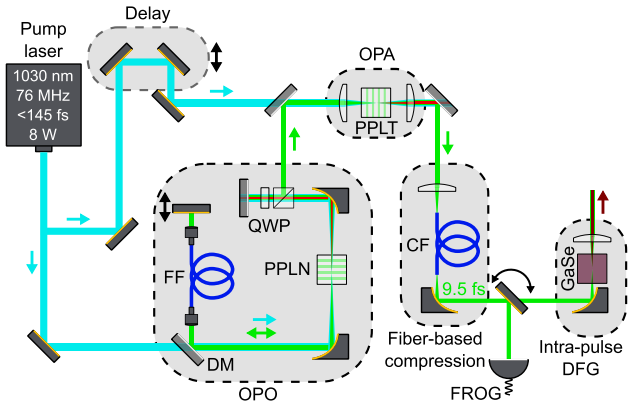

Fig. 1. Schematic setup of the experiment. The optical elements are QWP, quarter-wave plate; FF, feedback fiber; DM, dichroic mirror; CF, compression fiber; PPLN/PPLT, periodically poled lithium niobate/tantalate; OPO/OPA, optical parametric oscillator/amplifier; and DFG, difference frequency generation. The fiber-based compression can generate an average power of up to 620 mW at 1600 nm with a sub-two optical cycle pulse duration.

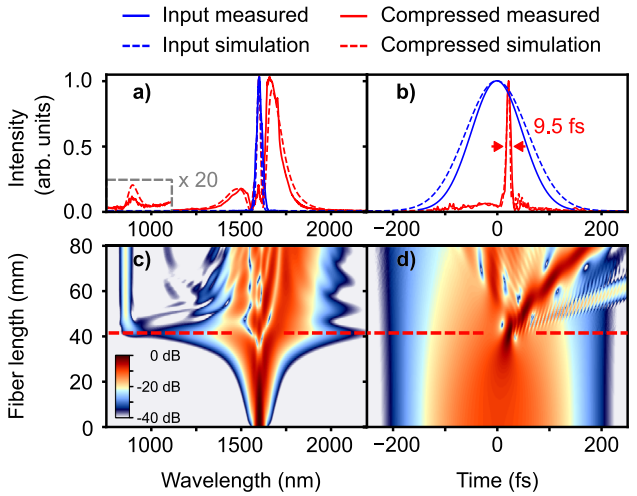

Fig. 2. For the shortest pulse achieved, the simulated [27] and measured spectral and temporal intensities are shown in (a) and (b), respectively. The 20 times magnified inset shows the dispersive wave. The simulated spectral (c) and temporal (d) field evolution of the pulse traveling along the compression fiber are also illustrated. The dashed red line marks the shortest temporal duration during the propagation.

leading edge slows down compared to the trailing edge and the pulse experiences adiabatic nonlinear temporal compression [24,25]. The full description of this process is given by the generalized nonlinear Schrödinger equation (GNLSE) [26]. The GNLSE is solved for the experimental parameters using PyNLO [27] and shown in Fig. 2. One clearly sees in Fig. 2(d) the temporal evolution to the shortest possible duration as the pulse travels along the fiber. After this point, soliton dynamics lead to an increasingly complicated temporal pulse shape. The spectral evolution in Fig. 2(c) depicts the corresponding increase in spectral width up to the shortest duration after which the dispersive wave separates. The subsequent spectral evolution is characterized by the stable propagation of the dispersive wave, a periodic change in spectral intensity similar to higher-order soliton propagation and the soliton self-frequency shift of the spectrum toward higher wavelengths. The latter, in combination with the anomalous dispersion, leads to the accompanying temporal shift in Fig. 2(d).

The optical setup is shown schematically in Fig. 1. A commercial shot-noise-limited Yb-based pump laser (FLINT, Light Conversion Ltd.) serves as an initial pulse source. It provides sub-145 fs pulses at 1030 nm with a repetition rate of 76 MHz and up to 8 W of average power. The shot-noise limit is reached for frequencies higher than 600 kHz at a photo current of 20 mA. This was measured with the laser running at the maximum output power and 36 mW split off onto the detector. A fiber-feedback optical parametric oscillator (FFOPO) and OPA combination is chosen to implement the frequency conversion to 1600 nm. The FFOPO [28] is characterized by its broad tuning range and high stability. To use the FFOPO as a compact seeder, a small focal spot inside a 2-mm-long periodically poled lithium niobate (PPLN) crystal is chosen. This allows to generate a sufficiently high seed power using less than 1 W of the available pump and ensures a compact FFOPO cavity. The high-gain bandwidth of the short PPLN crystal results in sub-120 fs pulses from the FFOPO, which is slightly shorter than the pump pulse duration [29]. The seed is then amplified to around 900 mW using an OPA with a 3-mm-long periodically poled lithium tantalate (PPLT) crystal. This is achieved while preserving the pulse duration and keeping the beam profile Gaussian for a high fiber coupling efficiency. The signal is then coupled into a 42-mm-long piece of common single-mode silica fiber (PM1550-XP, Coherent). Coupling 620 mW into the fiber leads to a compression of the pulse duration from 116 fs to 9.5 fs. After the compression fiber, the ultrashort pulses are characterized using a home-built second-harmonic generation frequency-resolved optical gating (SHG-FROG) [30] setup, which was checked against an autocorrelator (APE Mini TPA) and utilizes only reflective optics except for the nonlinear β-BaBO4 (BBO) SHG crystal. The ultrashort pulses can also be used for MIR generation. The MIR generation is based on intra-pulse DFG, and the simple setup consists of an off-axis parabolic (OAP) mirror focusing the pulses inside a gallium selenide (GaSe) crystal. Tuning the phase-matching angle of the GaSe crystal allows to tune the central wavelength of the broadband MIR emission spectrum with up to 320 µW of average power at a central wavelength of around 9 µm and a full width at half maximum (FWHM) bandwidth of over 2 µm. This is achieved using easily available GaSe rather than more efficient but highly specialized orientation-patterned gallium phosphide.

By utilizing fan-out crystals in the FFOPO and OPA stages, the setup can be modified to allow for a broadly tunable central wavelength. The fiber-based self-compression mechanism is also insensitive to a change in the central wavelength of the applied pulse, as long as it is larger than the zero-dispersion wavelength. Therefore, our architecture allows, in principle, for an ultrashort pulse with a central wavelength tunable by tens of nanometers, possibly up to over 100 nm.

The simulated spectral (Fig. 2(c)) and temporal (Fig. 2(d)) evolution of the pulse along the fiber for our experimental parameters are displayed in Fig. 2. A red dashed line marks the length of the compression fiber used in the experiment. After this length, the pulse duration has reached its minimum, and the simulated spectrum (Fig. 2(a)) and temporal duration (Fig. 2(b)), as well as their measured counterparts, are plotted in comparison to

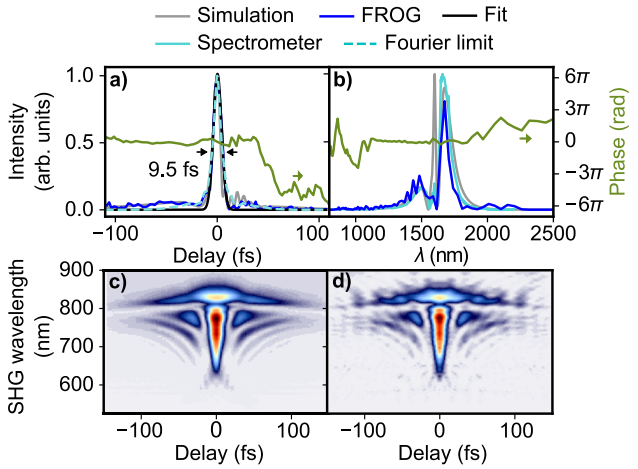

Fig. 3. Characterization of the pulses after the compression fiber. (a) Temporal pulse intensity and phase, retrieved using a home-built SHG-FROG, compared to the simulated [27] pulse duration. (b) Measured, simulated, and retrieved spectral intensity and phase. (c) Measured and reconstructed (d) FROG traces. The retrieved pulse duration of 9.5 fs is close to the Fourier limit of 9.2 fs. Above 60% of the pulse intensity is contained within the main pulse constrained by the black fit function.

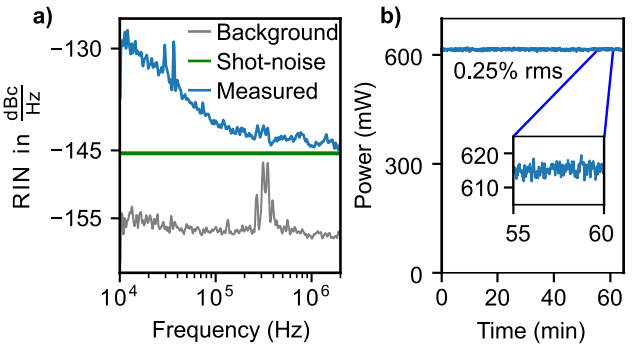

Fig. 4. (a) Measured relative intensity noise (RIN) of the compressed pulse train compared to the shot-noise limit at a photo current of 0.1 mA. The background demonstrates the noise of the detector without incident laser radiation. (b) Power stability of the compressed sub-two-cycle pulse over 1 h with a 5 min inset.

their initial values. Here one can clearly see the large compression factor of over 12 from 116 fs to 9.5 fs. Furthermore, the simulated and measured pulse durations agree well. The simulated and measured spectra also match closely, in particular the dispersive wave peaks displayed in the magnified inset to Fig. 2(a). When building this compressor, it is difficult to cut the fiber to the exact length required. One remedy for this is to vary the power coupled into the fiber. Doing so moves the point of shortest temporal duration along the fiber. Therefore, the shortest pulse duration for the specific fiber length can be achieved.

The measured and reconstructed FROG traces [31] used to determine the pulse duration are illustrated in Figs. 3(c) and 3(d), respectively. Even before retrieval, the FROG trace suggests a pulse with low chirp and most of its energy contained within a narrow temporal region. The reconstructed trace shares all important features with the measured trace. In combination with the FROG G error of 1.2%, this serves to validate the measurement. Simulated, measured, and retrieved spectra are depicted in Fig. 3(b). They agree well in shape except for the narrow central peak predicted by the simulation. Figure 3(a) proves that the simulated pulse duration, the Fourier-limited pulse duration of the measured spectrum, and the retrieved pulse duration from the FROG measurement are all approximately 10 fs long. A Gaussian fit to the temporal pulse shape retrieved from the FROG measurement is 9.5 fs long and therefore close to the 9.2-fs-long Fourier limit. This small difference is well within the expected range for FROG measurements of few-cycle pulses [32]. As such, the pulse duration is Fourier-limited, which is also indicated by the flat spectral and temporal phase in Fig. 3. It should be noted that two spectrometers (Yokogawa AQ6375, Ando AQ-6315E) were needed to cover the spectral range of the pulse. The temporal shape of the pulse also reveals that it has little secondary features and over 60% of its intensity is contained within the main peak. The clean temporal shape is a substantial advantage over systems based on erbium-doped fiber amplifiers at a similar center wavelength [12]. They show significant afterpulsing rather than a single main peak. Moreover, erbium-fiber technology is limited in average power, while power scaling of the presented approach is straightforward by utilizing a higher power pump laser and a shorter fiber.

Figure 4(a) demonstrates the excellent noise properties of the laser presented in this Letter. The system exhibits shot-noise-limited performance for frequencies higher than 300 kHz. A low-noise transimpedance amplifier detector circuit with an InGaAs photodiode (Hamamatsu G12182-003K) and a 10 MHz high-pass filter in combination with a lock-in amplifier (Zurich Instruments MFLI) were used to measure the RIN. The detector's background noise, acquired with the laser blocked, is much smaller than the shot-noise for the used photo current of 0.1 mA and frequencies over 10 kHz. The excellent stability is also reflected by its 0.25% rms power noise measured over 1 h and shown in Fig. 4(b).

To expand the capabilities of this laser system, a virtually alignment-free intra-pulse DFG stage using a 1-mm-thick GaSe crystal was added, producing ultrabroadband MIR radiation. Figure 5 reveals that the DFG spectra span most of the molecular fingerprinting region from 4 μm to over 12 μm and therefore exceed the measurement range of our spectrometer (FTIR Rocket, Arcoptix S.A.). The tuning range of the center wavelength, through variation of the phase-matching angle, also spans several micrometers in wavelength. Up to 320 μW output power at a central wavelength of around 9 μm and a FWHM bandwidth of over 2 μm are achieved with this system and make it suitable for many spectroscopic applications. The suitability of the source for the latter can be seen by the presence of strong water absorption lines in the 6 μm region. The intra-pulse DFG could easily be set up inside an enclosure, which can be nitrogen flooded or filled with a gas to be sampled. This means that there is no need to flood the entire setup with nitrogen gas to prevent unwanted absorption lines in the MIR. The weak secondary peaks in the intra-pulse DFG spectra are possibly the first sidelobes of the phase-matching spectrum caused by wave vector mismatch.

Most commercial broadband MIR sources are based on complex soliton dynamics that are inherently noisy [33,34]. The noise can be somewhat improved by adding a short piece of a

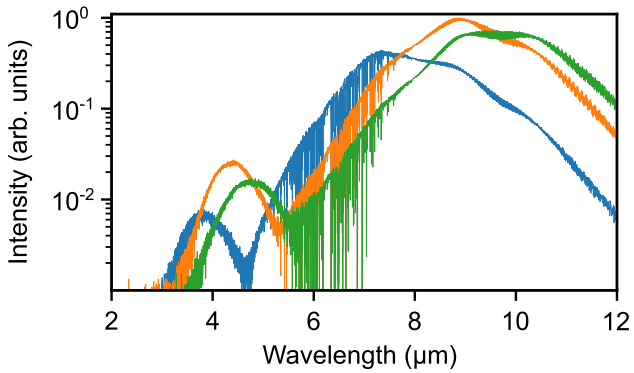

Fig. 5. Intra-pulse DFG spectrum spans several micrometers and is tunable over an even broader range by varying the phase-matching angle of the GaSe crystal. Each trace shown is the DFG signal for a different phase-matching angle. This system is capable of producing up to 320 μW mid-infrared average power. In the spectral range between 5 μm and 7 μm, water absorption lines are visible.

normal dispersion fiber [33]. We avoid this noise source by cutting the compression fiber shortly before the soliton fission point. The coverage of the MIR spectral region is then achieved through intra-pulse DFG. As a phase-sensitive optical parametric process, this only adds minor noise to the proven ultralow-noise properties of the presented few-cycle pulse source [35,36].

In conclusion, we have demonstrated a compact and very stable laser source of two-cycle pulses centered around 1600nm with an average power of 620 mW and at a 76 MHz repetition rate. The combination of ultrashort pulses and a demonstrated low RIN is a unique feature of this system and makes it attractive for high-precision time-resolved measurements. Furthermore, we prove that the system can also serve as a tunable broadband mid-infrared source, which may be applied to trace gas detection [37] and plasma analysis [38] using Fourier transform spectroscopy. This laser system can be implemented in ultrafast laboratories from easily available commercial components and as such can serve as a radiation source for many applications such as ultrafast spectroscopy [8] and molecular fingerprinting [12].

Funding. Bundesministerium für Wirtschaft und Klimaschutz (Zentrales Innovationsprogramm Mittelstand); Carl-Zeiss-Stiftung; Deutsche Forschungsgemeinschaft (431314977/GRK2642); Center for Integrated Quantum Science and Technology (IQST); Baden-Württemberg Stiftung; Bundesministerium für Bildung und Forschung (KMU MIRSWEEP); Ministerium für Wissenschaft, Forschung und Kunst Baden-Württemberg (Innovationscampus Mobilität der Zunkunft).

Disclosures. HG: Stuttgart Instruments GmbH (I,E); TS: Stuttgart Instruments GmbH (I,E); JT: Stuttgart Instruments GmbH (E).

Data availability. Data underlying the results presented in this Letter are not publicly available at this time but may be obtained from the authors upon reasonable request.

REFERENCES

1. U. Keller, Nature **424**, 831 (2003).
2. U. Morgner, Nat. Photonics **4**, 14 (2010).
3. G. Steinmeyer, D. H. Sutter, L. Gallmann, *et al.*, Science **286**, 1507 (1999).
4. R. Huber, S. Spörlein, J. E. Moser, *et al.*, J. Phys. Chem. B **104**, 8995 (2000).
5. S. Keiber, S. Sederberg, A. Schwarz, *et al.*, Nat. Photonics **10**, 159 (2016).
6. P. Sulzer, K. Oguchi, J. Huster, *et al.*, Phys. Rev. A **101**, 033821 (2020).
7. R. Huber, F. Tauser, A. Brodschelm, *et al.*, Nature **414**, 286 (2001).
8. M. Maiuri, M. Garavelli, and G. Cerullo, J. Am. Chem. Soc. **142**, 3 (2020).
9. D. Polli, P. Altoè, O. Weingart, *et al.*, Nature **467**, 440 (2010).
10. G. Cerullo and S. De Silvestri, Rev. Sci. Instrum. **74**, 1 (2003).
11. C. Erny, K. Moutzouris, J. Biegert, *et al.*, Opt. Lett. **32**, 1138 (2007).
12. H. Timmers, A. Kowligy, A. Lind, *et al.*, Optica **5**, 727 (2018).
13. D. M. B. Lesko, H. Timmers, S. Xing, *et al.*, Nat. Photonics **15**, 281 (2021).
14. C. Gaida, M. Gebhardt, F. Stutzki, *et al.*, Opt. Lett. **40**, 5160 (2015).
15. S. Xing, D. M. B. Lesko, T. Umeki, *et al.*, APL Photonics **6**, 086110 (2021).
16. R. Paschotta, Opt. Express **18**, 5041 (2010).
17. J. Zhang, K. Fritsch, Q. Wang, *et al.*, Opt. Lett. **44**, 2986 (2019).
18. D. Brida, M. Marangoni, C. Manzoni, *et al.*, Opt. Lett. **33**, 2901 (2008).
19. A. Grupp, A. Budweg, M. P. Fischer, *et al.*, J. Opt. **20**, 014005 (2017).
20. C. Homann, C. Schriever, P. Baum, *et al.*, Opt. Express **16**, 5746 (2008).
21. A. Steinmann, A. Killi, G. Palmer, *et al.*, Opt. Express **14**, 10627 (2006).
22. L. Qiu, M. Sun, X. Xie, *et al.*, Opt. Express **32**, 7633 (2024).
23. S. Boivinet, P. Morin, J.-P. Yehouessi, *et al.*, *Laser Congress 2019 (ASSL, LAC, LS&C)* (Optica Publishing Group, 2019), paper ATh2A.6.
24. L. F. Mollenauer, R. H. Stolen, and J. P. Gordon, Phys. Rev. Lett. **45**, 1095 (1980).
25. B. Sierro, P. Hänzi, D. Spangenberg, *et al.*, Optica **9**, 352 (2022).
26. J. Hult, J. Lightwave Technol. **25**, 3770 (2007).
27. Y. Casg, D. Hickstein, P. Ynlo, *et al.*, "pyNLO, Nonlinear optics modeling for Python," Github (2024), https://github.com/pyNLO/PyNLO.
28. T. Steinle, F. Mörz, A. Steinmann, *et al.*, Opt. Lett. **41**, 4863 (2016).
29. A. Alabbadi, T. Steinle, and H. Giessen, Opt. Lett. **47**, 3099 (2022).
30. K. W. DeLong, R. Trebino, J. Hunter, *et al.*, J. Opt. Soc. Am. B **11**, 2206 (1994).
31. Trebino group, "Code for retrieving electric field from FROG trace," https://frog.gatech.edu/code.html (2024).
32. J. Zhang, K. Fai Mak, N. Nagl, *et al.*, Light: Sci. Appl. **7**, 17180 (2018).
33. R. E. Hansen, C. R. Smith, A. Moltke, *et al.*, Laser Photonics Rev. **17**, 2200776 (2023).
34. J. M. Dudley and S. Coen, Opt. Lett. **27**, 1180 (2002).
35. Q. Bournet, M. Natile, M. Jonusas, *et al.*, Opt. Express **31**, 12693 (2023).
36. K. Bencheikh, E. Huntziger, and J. A. Levenson, J. Opt. Soc. Am. B **12**, 847 (1995).
37. A. Khodabakhsh, R. Krebbers, K. van Kempen, *et al.*, in *Optica Sensing Congress 2023 (AIS, FTS, HISE, Sensors, ES)* (Optica Publishing Group, 2023), paper ETu5E.1.
38. R. Krebbers, N. Liu, K. E. Jahromi, *et al.*, Sci. Rep. **12**, 9642 (2022).